OPEN ACCESS

Int. Jr. of Contemp. Res. in Multi. *PEER-REVIEWED JOURNAL* *Volume 4 Issue 4 [Jul- Aug] Year 2025*

Research Article

Synthesis And Characterization of Sphere Like Copper Oxide and Its Electrocatalytic Performance for The Selective Determination of Paracetamol in Biological Samples

Palpandi Karuppaiah
Vadasithur, Coimbatore District, Tamil Nadu-641202, India

Corresponding Author: *Palpandi Karuppaiah

DOI: https://doi.org/10.5281/zenodo.16732259

Abstract

Synthesis of nanomaterials for efficiently detecting pharmaceutical medicaments such as paracetamol (PRC) is important for industrial and pharmacological applications. In this study, we prepared copper oxide nanospheres (CuO-NSPs) via facile chemical co-precipitation along with the sonochemical technique. The prepared CuO-NSPs were fabricated on a disposable screen-printed carbon electrode (SPCE) utilized for conducting sensitive and selective electrochemical detection of PRC. The CuO-NSPs were systematically characterized using various spectroscopic techniques, including X-ray diffraction, Fourier transform infrared spectroscopy, energy dispersive X-ray analysis, field emission scanning electron microscopy, and Raman spectra. The electrochemical properties of CuO-NSPs were verified using electrochemical impedance spectroscopy (EIS), Cyclic voltammetry (CV) and linear sweep voltammetry techniques. As an electrochemical sensor, the proposed sphere-like copper oxide screen printed carbon electrode (CuO-NSPs/SPCE) demonstrated an excellent sensitivity with a wider linear response range from 0.01 to 1480µM. The electrode also has good sensitivity. Different coexisting compounds were present when the selectivity was tested. Last but not least, the CuO-NSPs/SPCE consistently demonstrates reproducibility, durability, and other critical aspects for future development as a point-of-care device.

Manuscript Information

- **ISSN No:** 2583-7397
- **Received:** 21-06-2025
- **Accepted:** 27-07-2025
- **Published:** 03-08-2025
- **IJCRM:**4(4); 2025: 386-395

- **Plagiarism Checked:** Yes
- **Peer Review Process:** Yes

How to Cite this Article

Karuppaiah P. Synthesis And Characterization of Sphere Like Copper Oxide and Its Electrocatalytic Performance for The Selective Determination of Paracetamol in Biological Samples. Int J Contemp Res Multidiscip. 2025;4(4):386-395.

Access this Article Online

www.multiarticlesjournal.com

KEYWORDS: Copper oxide nanospheres, facile approach, Cyclic voltammogram, electroanalysis, paracetamol determination, pharmaceutical and biomedical applications

1. INTRODUCTION

Metal oxide nanostructures are crucial materials for magnetic storage media, solar energy conversion, electronics, and catalysis. Some transition metal oxides, such as zinc oxide, titanium dioxide, and iron oxide, have been proven to be potential candidates for many applications. Among all transition metal oxides, copper oxide (CuO) is categorized as a highly attractive metal oxide semiconductor material because of its superior performance in electronic and optoelectronic industrial applications such as gas sensing device fabrication, semiconductor, and thin films for photovoltaic cells [1-3]. Copper oxide is a readily accessible and non-toxic substance. The narrow band gap energy of CuO is 2.0 eV [4]. Furthermore, the fabrication and processing of CuO entails low cost [5,6]. Several synthetic approaches have been recently reported for the preparation of different CuO nanostructures such as thermal oxidation of copper foil, hydrothermal synthesis, vapor-phase solid preparation, and ultrasonic irradiation Methods, thermal breakdown of precursors, electrodeposition, and electron beam lithography [5-11]. Nonetheless, it remains a problem to devise a straightforward, quick, easily controllable, and energy-efficient process for the large-scale production of CuO nanostructures with customizable shape. As of now, numerous morphological CuO nanostructures have been synthesized via straightforward solution methods, including ribbon-like films [12], nanowires [13], nanorods [14-28], plate-like powders [19], hollow microspheres [20], 3D bundles of CuO nanorods and nanowires [21-22], hierarchical flower-like CuO films [6, 23], and butterfly-like CuO [24] and more nanostructures.

Paracetamol (PRC; N-acetyl-p-aminophenol) is a pain reliever and fever reducing agent [25-26]. It acts by inhibiting the release of certain chemical messengers that produce pain and heat. Paracetamol was commonly utilized during the 1950s. PRC is still widely used as a pain reliever over the world. According to the national health service, adults should take the appropriate amount of 500mg (2 tablets/day), while children (age 16 and under) should take 500mg (1 tablet/day). If they It works better than aspirin as a pain reliever for headaches, backaches, arthritis, and post-operative pain [27-28]. PRC seldom produces negative effects when used at the recommended dosage. In general, PRC appears to be harmful even when eaten in regular therapeutic levels, and it can cause major side effects such as hepatotoxicity and nephrotoxicity, which are associated with liver and kidney damage [29-30]. Few months ago, indian government (Karnataka) banned the paracetamol (650 mg) due to its higher side effects. As a result, the development of a simple, rapid, sensitive, and accurate approach for determining PRC is critical for pharmaceutical quality control and overdose detection [29-32].

As per previous studies, numerous techniques have been utilized for quantifying PRC in biological fluids and pharmaceutical formulations such as chromatography [33], capillary electrophoresis [34], spectrophotometry [35], flow injection methods [36], and electroanalytical techniques. The electrochemical technique is more efficient than all aforementioned methods and is the most widely applied because it has the following characteristics: higher sensitivity, good selectivity, quick response, easier to operate, and inexpensive [37-41,42, 60-62].

In the present research paper, we report a facile chemical precipitation method with sonication for the preparation of CuO-NSPs. For the first time we have attained this approach to prepare sphere-like copper oxide nanostructures without using modifiers and surfactants and so on. The formation of CuO-NSPs reaction mechanism was detailed. We have fabricated the CuO-NSPs modified screen-printed carbon electrode without utilizing of linkers and the paracetamol electrochemical sensing properties of CuO-NSPs/SPCE electrodes were systematically studied.

1. Experimental Details

1.1. Chemicals and Apparatus

Copper sulfate heptahydrate ($CuSO_4.7H_2O$), sodium hydroxide (NaOH), and paracetamol (PRC) were purchased from Sigma-Aldrich. All the chemicals were used as received, and phosphate buffer was prepared using purified water. The as-synthesized compound was well characterized by using the pattern obtained from an X-ray diffractometer (PAN analytical, Netherlands), field emission scanning electron microscope (JSM-7610F), Raman spectroscopy and an energy dispersive X-ray analyzer (EDX-HORIBA EMAXX-ACT). Impedance studies were analyzed utilizing an electrochemical impedance spectroscopic technique (EIM6ex Zahner, Germany). The Cyclic voltammetric studies were conducted using equipment from CH Instruments, USA. An electrochemical analyzer (CHI115A, CH Instruments) was employed for conducting Cyclic voltammograms and linear sweep voltammetry measurements.

1.2. Formation of CuO NSPs

Copper oxide (CuO) nanospheres were prepared through a simple chemical co-precipitation technique associated with probe-sonication [45]. Firstly, 3.5g of $CuSO_4.7H_2O$ was dissolved in 250-mL DD-water and mixed thoroughly. Moreover, 2.5g sodium hydroxide (NaOH) was dissolved in 100-mL DD-water individually. Then, the copper sulphate solution was transferred in a round-bottomed flask (RB-flask) conduct with a magnetic stirring at 650 rpm for 120 minutes. Subsequently, alkaline solution was added in a drop-wise manner (5mL/min) with constant stirring. To maintain the pH ranges from 8.0 to 11.5 at room temperature (25°C±). Afterwards, the solutions are subjected to sonication at 60W, 30 minutes under cold condition. The resulting of as-obtained brown color precipitate was consecutively washed with water until the pH reached at 6.5 to 7.0. Then, ethanol (99%) was used to purify the final product, and the mixture was centrifuged at 5000 rpm for 20 minutes thrice and filtered through a membrane filter (0.2µM). Afterward, the obtained products were dried in a lyophilizer at -60°C (-76 F) for 75 minutes and allowed to dry at 155°C in a hot air oven for 1 hour. Laterly, the product was calcined at 500°C for 1.5 hours and finely pulverized using an agate mortar with pestle.

Eventually, the electrochemical studies were conducted at room temperature on the prepared sample. Scheme 1. explored the preparation of CuO-NSPs and its electrochemical oxidation of PRC on CuO-NSPs/SPCE. The formation of CuO-NSPs and the chemical reaction are written in equations (1 and 2),

$$CuSO_4 .7H_2O_{(aq)} + 3NaOH_{(aq)} \rightarrow Cu(OH) + Cu(OH)_{2(S)} + 3NaSO_{4(aq)} \rightarrow (1)$$

$$Cu(OH) + Cu(OH)_{2(S)} \xrightarrow{\Delta} CuO_{(S)} + 3H_2O \rightarrow (2)$$

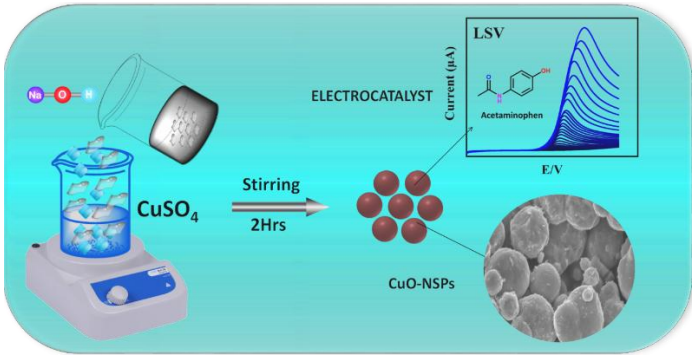

Scheme 1: Synthesis of CuO-nanospheres and its electrocatalytic applications

1.3. Preparation of CuO-NSPs modified screen printed carbon electrode (CuO-NSPs/SPCE)

To develop the PRC sensor, about 5 mg of CuO-NSPs was dispersed in 1-mL of DD-water, and allowed to sonicate for 90 min to form a homogeneous suspension. Then, 6 µL suspensions of CuO-NSPs were installed directly on the surface of the SPCE. Subsequently, the SPCE was left to dry in an oven at 70°C for 2 min. Therefore, additional electrochemical research was conducted using the manufactured electrode. Fig S1 explains the preparation of CuO-NPs modified SPCE.

1.4. Real sample preparation (Human urine)

A refrigerator was utilized to store human urine (HU) biological sample. Firstly, the urine sample was centrifuged at 5000 rpm for 30 mints and filtered through membrane filter (0.001nm). From this collected sample, known amount of PRC solution were spiked into a 50mL of volumetric flask containing HU and shaken well for few minutes. It is kept in a refrigerator at 4°C until the experiments. To quantify the PRC sample content, the standard addition method was implemented using Cyclic voltammetry technique (CV) in the presence of 0.1M PB solution, pH at 7.0. These analyses were conducted at an ambient temperature conditions.

1.5. Quantification of Paracetamol (PRC)

The electroanalytical behaviour of CuO-NSPs toward the oxidation of PRC was investigated through Cyclic voltammetry (CV) analysis containing 0.1 M PB solution (pH 7.0) at a scan rate of 0.05 Vs^{-1} at room temperature. Various concentrations of PRC ranging from 0 to 210 µM were detected using the modified electrodes, and the linear plot was used to calculate the peak current (µA) *versus* PRC concentrations (µM). To sustain the stability of the electrode, it is kept in a refrigerator at 4°C immersed in 0.1M PB solution.

2. Statistical data interpretation of CuO-NSPs

2.1. Morphological and composition analysis of CuO-NSPs

The surface morphological features of as-prepared copper oxide were confirmed by using field emission scanning electron microscopy (FE-SEM), and the images were recorded at different magnifications (Fig.1). Fig 1 (A-B) displays the FE-SEM micrographs of CuO-NSPs at different magnifications product shows a uniform structure comprising spherical-like morphology in huge quantities. The nanoparticles are homogeneously distributed and their size is not found in non-uniform. The average particle size distribution of the CuO-NSPs has been estimated by fitting the particle size distribution histogram to the long-normal distribution function, which is interpreted as the equation (3), [64],

$$f(D) = \left(\frac{1}{\sqrt{2\pi}\sigma_D}\right) \exp - ln^2 \left(\frac{D}{D_0}\right) / 2\sigma^2 \quad \rightarrow (3)$$

Here, D corresponds to the average particle size, and σ_D is the standard deviation. The estimated average size of the CuO-NSPs was found to be 65.19 nm, along with the standard deviation of 1.375nm (Fig. S2). After being cleaned with ethanol, the glass piece and copper coin were left to dry for a few minutes at 55°C in a hot air oven. Additionally, the drop-coated nanoparticles were dried using the newly indicated technique. Before characterization, the produced nanoparticles were combined with 99.99% ethanol and applied in a few drops to the surface of the glass piece that was coated to the copper coin. We employ this technique to remove contaminants from the nanoparticles and get a clear morphological structure. Fig S3 explains the drop coating technique.

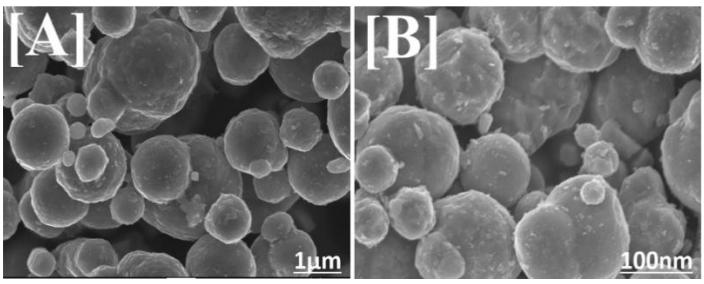

Fig. 1: FESEM morphograph of as-synthesized CuO-NSPs

Simultaneously, an energy dispersive X-ray (EDS) analysis was used to evaluate the CuO-NSPs, materials purity, the determination of elemental composition consisting within the materials before and after calcination process, as depicted in **Fig 2.** From CuO EDS spectrum, the presence of copper and oxygen elements in the CuO-NSPs, electrode were confirmed. These data indicated that the nanoparticles are merely stoichiometric **(Fig. 2 (A))**, and the weight percentages of Cu

and O in the CuO, calculated using EDS results, were 21.0% (Oxygen) and 79.0% (Copper), respectively.

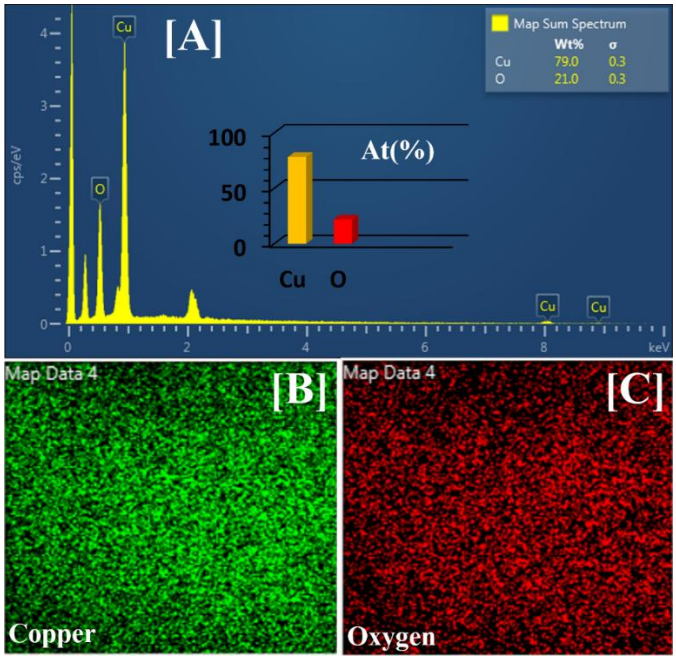

Fig. 2: EDS spectrum of CuO-NSPs (Inset with corresponding EDX scaling of location) (A), and Elemental mappings (B-C).

To determine the location of copper and oxygen, an elemental mapping was carried out. The results are shown in Fig. 2. From the Fig 2. (B) And (C) Copper (Cu) and oxygen (O) elements are localized within the CuO-NSPs was confirmed.

2.2. Crystalline structure analysis of CuO-NSPs

Using X-ray diffraction (XRD), the crystalline structure and phase purity of CuO-NSP electrodes were described in Figure 3. After calcining the precipitate at 500°C, the XRD pattern of CuO-NSPs is shown in (A). The prominent diffraction peaks of CuO-NSPs observed at 32.48°, 35.54°, 38.78°, 48.78°, 53.35°, and 58.23° corresponding to the ($\bar{1}10$), ($\bar{1}11$), (022), (111), (202), (020), and ($\bar{1}13$) planes respectively. These XRD patterns can be attributed to the monoclinic crystalline CuO-NSPs, which is in agreement with the standard JCPDS data (ref no:89-2531). No other characteristic peaks of impurities such as $Cu(OH)_2$, or precursors were observed, thus indicating the formation of a pure phase CuO-NSPs. The average crystallite of CuO-NSPs was examined using the full-width half maximum (FWHM) value of the prominent diffraction peak of the XRD pattern through Scherer's equation (4) as follows [44], and the FWHM observed peak is represented in Fig. S4.

$$X_s = k\lambda/\beta \cos\theta \quad \rightarrow \qquad (4)$$

Where Xs represents the crystal size, λ denotes the wavelength of the X-ray, ß signifies the full width at half maximum (FWHM) of the diffraction peak (observed value β = 0.54832), and θ is the angle of diffraction, and k is Scherer's constant. The crystal size was calculated from the diffraction plane ($\bar{1}11$), and the average crystalline size of the CuO-NSPs was found to be 15.4nm, with the calculated lattice micro strain (ϵ) is 0.00740, and the formula is described in Fig S5. The experimental results were similar to the diffraction patterns of CuO-NSPs reported in a previous literature [45]. Additionally, the crystal structure of the as-synthesized pure CuO unit cell is depicted in Fig S10.

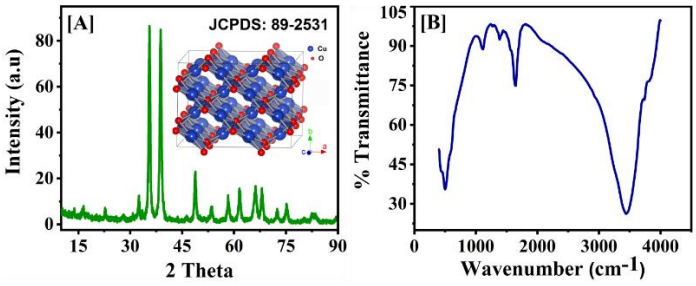

Fig. 3: Illustrative results of XRD pattern for CuO-NSPs and FTIR spectrum.

To determine the chemical and structural nature of the synthesized CuO-NSPs, the effect of chemicals used, Fourier transform infrared spectroscopy (FTIR) analysis was used. Fig 3 (B) depicts the IR spectrum recorded for the CuO-NSPs, in the range of 400-4500 cm^{-1}. As the prepared CuO nanospheres, the FTIR spectra (Figure. 3 (B) shows bands at around 495.55, 1108.07, and 1386.11 cm^{-1}, which can be assigned to the vibrations of Cu-O bonds. There is sharp peak observed at 1644.66 cm^{-1} in the spectrum CuO nanoparticles which is the characteristics of Cu-O bond formation. The broad absorption peak at around 3436.04 cm^{-1} (-OH) is caused by the adsorbed water molecules since the nano crystalline materials exhibit a high surface to volume ratio and thus absorbs moisture.

Additionally, In order to investigate the band gap energy of as prepared CuO-NSPs nanoparticles were examined by UV-Vis spectrophotometer and the results are shown in Fig S6 (A-B) and the energy band gap was calculated from Tauc's formula which shows the relationship among absorption coefficient and the incident photon energy of CuO-NSPs. The Tauc's equation (5) is presented as below;

$$\alpha h\upsilon = A\,(h\upsilon - E_g)^{n/2} \quad \rightarrow (5)$$

Where α is the absorption coefficient, A is a constant, and n depends on whether the transition semiconductor is indirect (n=4) and direct (n=1). where A is a constant, n is dependent on whether the transition semiconductor is direct (n=1) or indirect (n=4), and α is the absorption coefficient. Accordingly, plotting $(\alpha h\upsilon)^2$ as a function of hυ has been displayed in Fig S6 (A-B). The linear absorption edge of the curve may be used to extrapolate the direct band gap energy. The E_g of CuO-NSPs was found to be 1.24 eV. When the band gap decreased from the transition energy showed an obvious red shift. The obtained absorbance energy of the CuO nanoparticle is 358.23nm. Furthermore, Figure S11 depicts the Raman spectrum analysis

of as-prepared CuO nanoparticles. It represents the measured CuO peaks at 1420 cm^{-1} (D band) and 1569 cm^{-1} (G band), respectively. This database confirmed the development of CuO nanoparticles.

3.3 Electrochemical properties of CuO NSPs/SPC electrode

The electrochemical impedance spectroscopy (EIS) results of the unmodified SPCE and modified electrodes (CuO-NSPs) in 0.1M KCl containing 5mM $Fe(CN)_6^{3-/4-}$ at room temperature were shown in Fig. 4. An applied frequency range was fixed at 100MHz to 100KHz. Figure 4 displays the rate of charge transfer reaction on the surface of bare SPCE and CuO-NSPs modified SPCE. The CuO-NSPs' narrower semicircle curve suggests a lower impedance value, facilitating simpler electron transmission [46-48]. The Randles equivalent circuit model is displayed in inset Fig 5. In order to suit the Nyquist plot, this model makes use of electrolyte resistance (R_s), charge transfer resistance (R_{ct}), double layer capacitance (C_{dl}), and Warburg impedance (Z_w). Compared to the unmodified SPC electrode, the semicircle section of the EIS plot acquired for CuO-NSPs/SPCE was 2.4 times greater. For the naked SPCE (Fig. 4(a)), the equivalent R_{ct} values were 1740.15, and for CuO-NSPs (Fig. 5(b)), they were 530.22 for CuO-NSPs (Fig 5(b)) respectively. These results from the impedance analysis suggested that CuO-NSPs are good conductive materials for constructing an electrochemical sensor.

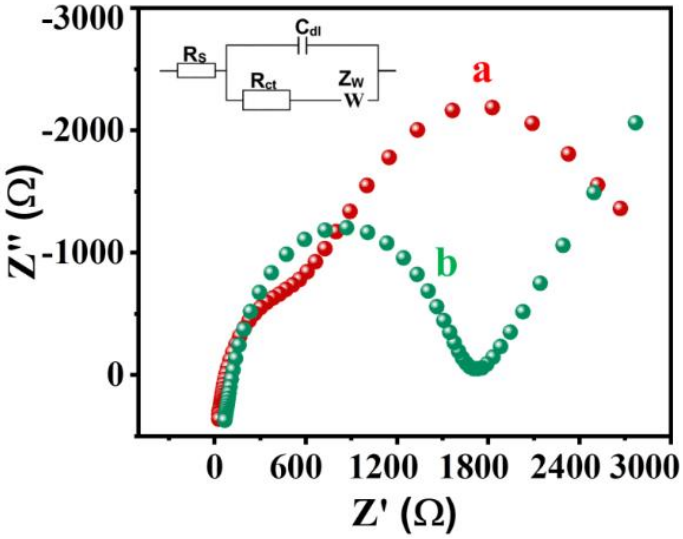

Fig 4: Typical Nyquist semicircle plots of EIS spectra.

Electrode fabrication step measured in a mixture of 5mM of $Fe(CN)_6^{3-/4-}$ and 0.1M KCl solutions at an applied amplitude of ±5mV within a frequency range of 0.01Hz-100MHz. Curve **(a)** Bare SPCE and **(b)** CuO NSPs modified SPCE. Randles equivalent circuit model is shown in inset.

3.4. Quantification of PRC at CuO-NSPs/SPCE

The electrocatalytic oxidative properties of paracetamol (PRC) obtained using the unmodified SPCE and the CuO-NSPs/SPCE was studied utilizing 0.1M PB solution (pH 7.0) at a scan rate 0.05Vs^{-1} by conducting Cyclic voltammetry (CV) tests. The bare SPC electrode shows the small oxidation peak at 0.52V in the presence of PRC (Fig. 5A (a)), which indicates that the bare SPCE is electrochemically active with little response current and it is not more favorable for the detection of PRC in the selected potential range. Conversely, when the unmodified SPCE was grown with CuO-NSPs (10µM PRC), a strong oxidation behaviour with the peak potentials of 0.45V was obtained (Fig. 5A (b)). The oxidation peak current of PRC obtained using CuO-NSPs/SPCE was due to the oxidation processes that occurred, because of two electrons and one proton transfer. The possible electrocatalytic oxidation mechanism of PRC at CuO-NSPs/SPCE is illustrated in the Scheme 2. Moreover, the oxidation peak current obtained by CuO-NSPs modified electrode was 1.5- fold higher than that of bare SPCE. This result proved that the CuO-NSPs/SPCE had excellent electrocatalytic activity. The catalytic features of the sensor may be due to their unique properties of CuO-NSPs electrodes, such as high-volume ratio, large surface area and subtle electronic characters. Furtherly, the catalytic properties of this sensor device was confirmed by conducting CV analysis by varying the concentration of PRC ranges from 0 to 210µM in the presence of supporting electrolyte 0.1M PB solution (pH 7.0) at a sweep rate of 0.05Vs^{-1}, as shown in **Fig 5 (B)**. The corresponding linear plot obtained from the relationships of oxidation peak current versus PRC concentration is depicts in **Fig 5 (C)**. From this plot, the oxidation peak current significantly increases with increasing of PRC concentrations. To calculate the limit of detection, limit of quantification, selectivity and sensitivity, the CuO-NPs/SPCE was selected as a working electrode for further electrochemical investigations, and the oxidation peak was utilized as the analytical signal in linear sweep voltammetry (LSV) analysis due to its higher sensitivity. The electrochemical oxidation reaction was takes place at the modified electrode surface is represented as the equation (6) as follows:

$$2Cu^{2+} + C_8H_9NO_2 \rightarrow 2Cu + C_8H_7NO_2 + 2H^+ \qquad \rightarrow (6)$$

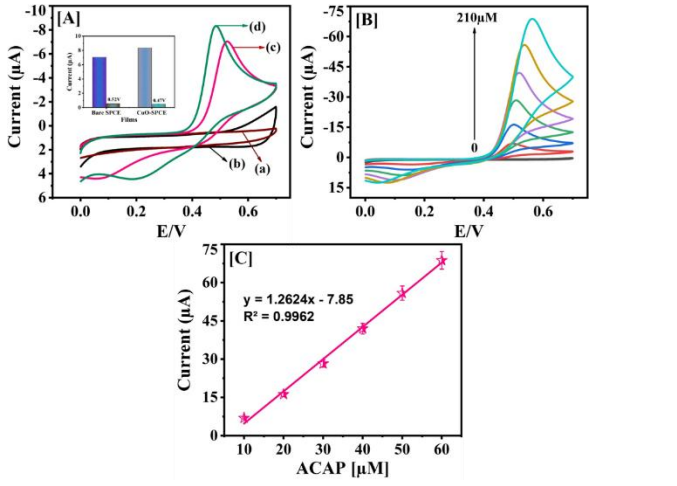

Fig 5 A. CV profiles of different films bare SPCE (a) and CuO-NSPs/SPCE (b). (B) CVs of CuO-NSPs/SPCE containing 0-210µM of PRC. Supporting electrolyte: 0.1M PB solution (pH 7.0) at a sweep rate 0.05Vs^{-1}. (C) Various concentration of PRC *vs.* peak current relationship.

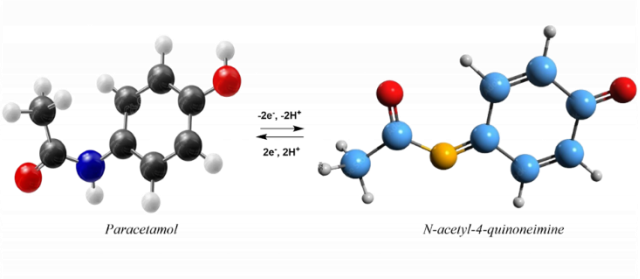

Scheme 2: Electrocatalytic oxidation of PRC at CuO-NSPs/SPCE

3.5. Impact of potential sweep rate on CuO-NSPs/SPCE

To further examine the electrochemical oxidation mechanism of PRC, the influence of scan rate (v) on the voltammetry response of PRC using CuO-NSPs/SPCE was studied in detail. Fig 6 (A) shows the CV analysis of CuO-NSPs/SPCE in 0.1M PBS (pH 7.0) with 10µM PRC (0.1mM) at scan rates ranging from 0.01 to 1.0 V/s^{-1}. A significant link between peak current and scan rate was discovered. The linear regression equations are illustrated in equations (7). Figure 6 (B) shows that the PRC redox reaction occurs at the CuO-NSPs/SPCE, indicating a diffusion-controlled mechanism.

I_{pa}/A = y= 0.026x + 8.9651 R^2-0.9946 → (7)

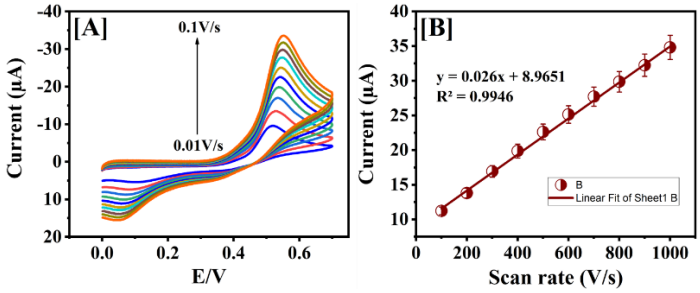

Fig 6 A. Various scan rates, (A) scan rates *vs*. current relationship (B).

Fig S7. Displays Tafel graphs demonstrating the relationship between redox potentials and log of various scan rates in seconds. The electron transfer coefficient can be computed using the slope value. On the reaction coordinate, the activated complex is located approximately midway between the reactants and products. In other words, the structure of an active complex reflects both reactants and products equally. The link between potential and log of scan rate is seen in equation (8) as follows:

I_{pc}/A=y=0.0299x +0.4607 R^2-0.9973 → (8)

Besides, the plots of E_p (anodic) *vs*. log υ exhibit the straight line with slopes of -2.3RT/(1-α)nF and -2.3RT/αnF for the E_{pa} [63]. Here, α and n_a (=2) are the electron transfer coefficient and number of electrons involved in the rate-determining step, while the constants R, T and F represent their usual meanings (R=8.314 J Kmol^{-1}, T=298K, F=96485C mol^{-1}). The charge transfer coefficient can be calculated from Tafel slopes. The value of α is 0.0299 (± 0.015), which is close to 0.5, means that the activated complex is around halfway between reactants and products on the reaction coordinate. In other words, the structure of the activated complex reflects reactants and products equally.

3.6. Analytical application of PRC sensor

Fig. 7 (A) displays the linear sweep voltammetry (LSV) curves obtained while using CuO-NSPs/SPCE toward the determination of paracetamol (PRC). For various concentrations of an analyte, a well-defined LSV response was observed. The oxidation peak of PRC increases with increasing concentration. The plot of the oxidation current *versus* PRC concentrations suggested good linearity with a linear regression of y=0.0531x + 0.2631 and R^2=0.9991, as presented in Fig. 7 (B). The obtained linear dynamic concentration ranges from 0.01µM to 1480 µM, and the sensitivity of the electrode shows 0.75857µA/µM^{-1} cm^{-2}. The limit of detection was calculated by the following equation (9);

$$LOD=3S_b/S \quad \rightarrow (9)$$

$$LOQ=10S_b/S \quad \rightarrow (10)$$

Where S_b is the standard deviation of the intercept of the regression line and S is denoted as the slope of the calibration curve. From the above equation, the calculated LOD was to be 0.01µM. The analytical characteristics, such as linear working range (LWR), sensitivity, and limit of detection (LOD), were compared to those in earlier research [49-59]. The comparison results are tabulated in Table 1. In addition, the obtained limit of quantification of the electrode (LOQ) shows 0.05757 and it is interpreted in equation (10). When compared with the other modified electrodes, which are presented in previous studies, the CuO-NSPs/SPC electrode is the simplest composite with higher sensitivity and a wide linear working concentration range. CuO-NSPs/SPCE is more suitable for future commercialization due to their facile synthesis compared with the electrodes described in previous literature.

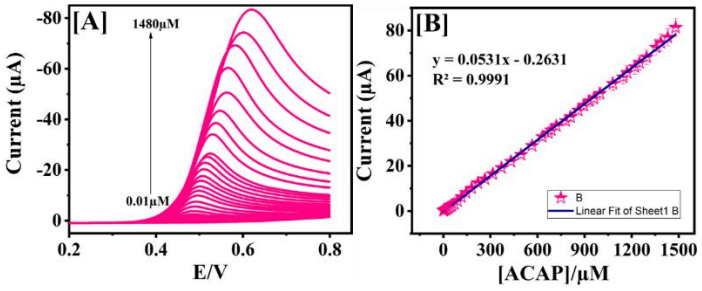

Fig 7: (A) LSVs of PRC at CuO-NSPs/SPCE and (B) corresponding linear plot for concentration *vs.* current.

Table 1: Comparison of the electrochemical sensors with current PRC sensor

Electrodes	Technique	LWR (µM)	Electrolyte (pH)	LOD(nM)	Sensitivity	Ref
[a]MWCNT/graphene/GCE	DPV	0.80-110.0	7.5	90	Nil	[49]
Graphene/[b]GCE	SWV	0.1-20	9.3	32	Nill	[50]
Boron-doped-diamond/E	DPV	0.5-83	4.5	490	Nill	[51]
MWCNT/[c]PPGE	SWV	0.1-25	7.5	45	Nill	[52]
Pyrolytic carbon electrode	DPV	15-225	7.0	1400	0.33	[53]
MoS_2-[d]GR	DPV	0.1-100	5.5	20	Nill	[54]
MWCNT/chitosan	DPV	1-145	3.0	10	Nill	[55]
Carbon nanotube paste/E	DPV	0.15-126	7.0	43	Nill	[56]
Carbon-coated-Ni-NPs	DPV	7.8-110	5.5	2300	Nill	[57]
Nafion/TiO_2-GR/GCE	DPV	1-100	7.0	2100	Nill	[58]
[e]PANI/ MWCNT/GCE	SWV	1-100	5.5	2500	Nill	[59]
Fe atoms	DPV	0.5-500	7.0	140	Nill	[65]
AuNPs/LIG	DPV	0.1-100	7.0	65	Nill	[66]
NiCo-MOF/CC	DPV	5-400	7.0	1000	Nill	[67]
SCB	IT	5-950	-	2500	Nill	[68]
CuO [f]NSPs/SPCE	LSV	0.01-1480	7.0	10	0.75857	This work

[a]MWCNT: multi-walled carbon nanotube, [b]GCE: glassy carbon electrode, [c]PPGE: plane pyrolytic graphite electrode, [d]GR: graphene, [e]PANI: poly aniline, [f]NWs: nanowires, [g]LOD: limit of detection, [h]µM: micromole, [i]nM: nanomole, [j]LWR: linear working range. E-electrode: SCB sugarcane bagasse biochar, IT-amperometry, Fe-(Iron), SPCE: screen-printed carbon electrode.

3.7. Precision, specificity, repeatability and storage stability analysis

To examine the specificity of the developed sensor was investigated in presence of some similar structure oxidizing chemicals and common ions such as 2-aminophenol (2-AP), 3-aminopehenol (3-AP), 4-aminophenol (4-AP), hydroquinone (HDQ), sulphate (SO_4^-), copper (Cu_2^+), glucose (GLU), catechol (CAT), and dopamine (DA), were the results are analyzed. Fig 8 (A) describes the LSV response of the CuO-NSPs/SPCE against 10µM of PRC and 20-fold higher concentration of interfering species (above mentioned). There is no significant interference was found for the detection of PRC. These results revealed that the electrode quickly responded to PRC (Fig. 8 (B)) and interfering substances. However, very quiet responses were observed when each interfering compound were injected separately (without PRC). This result suggests excellent selectivity of the CuO-NSPs/SPCE. As a result, the constructed sensor can be used in real-time to determine PRC.

The reproducibility was assessed in the presence of 0.1M PB solution (pH 7.0) containing 10µM of PRC, by CV method. Fig 8 (C) depicts the CV responses of PRC oxidation for 10 consecutive measurements. It can be seen that, a small variation was observed in the oxidation current for PRC for 10 measurements with the acceptable RSD 1.27%. Under the normal conditions at normal dosage, the entire paracetamol structure is quickly metabolized by undergoing glucuronidation and sulfation to inative metabolites which are excreted through urine. When intake of over dosing PRC, it interacts with alcohol and directly produce the high risk to liver and kidney, the excretion of PRC through the urine can be quantitatively determined. The metabolic activity and the excreton mechanism of PRC in human liver is clearly eluciated in Fig S8.

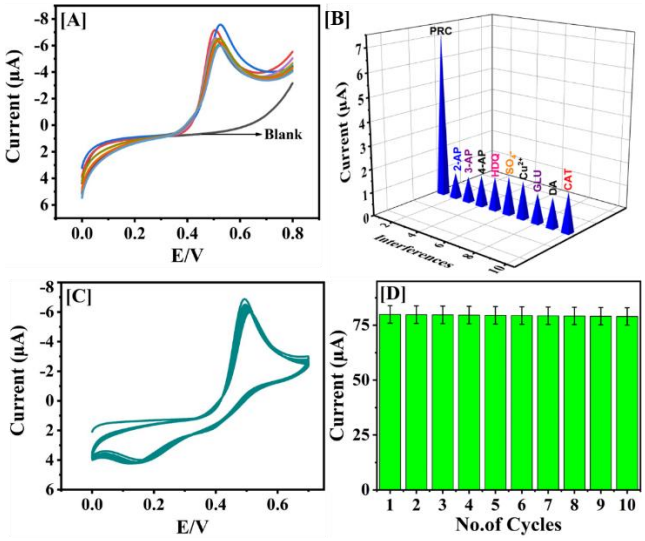

Fig 8 (A): Selectivity for the PRC at CuO-NSPs/SPCE in presence of 0.1M PB solution (pH 7.0). **(B)** Corresponding peak current *vs*. interfering species concentration.

3.8. Real sample analysis (Human urine)

In order to demonstrate the pragmatic applicability of the proposed sensor (PRC) were quantified in human urine (HU) on CuO-NSPs/SPCE. This sample was prepared before the experiment and three parallel determinations were carried out for this HU detection. Table. 1 presents the results. Consequently, the results obtained demonstrate the practical applications of the constructed sensor in actual samples, Fig S9.

Table 2: Quantification of PRC in real biological fluid

Samples	Added (µM)	Current (µA)
sample-1	1	1.741
sample-2	1	2.743
sample-3	1	3.969

4. CONCLUSION

To summarize the work, we have developed a technologically advanced electrochemical sensor for the effective selection and sensitization, to determine the paracetamol (PRC) which was constructed by green chemical synthesis of CuO-NSPs using a simple chemical co-precipitation with sonication method. These electrode materials' morphological characteristics were suitably and structurally described utilizing XRD, FTIR, EIS, Raman spectra and FE-SEM. The electrochemical property enhancement of the modified electrode toward the detection of PRC was confirmed by CV and LSV analysis. The experimental results suggests that the prepared electrochemical sensor showed an excellent specificity for the quantification of PRC in presence of potentially co-interfering compounds with a wide linear response range, lower limit of detection and good sensitivity. Due to this excellent behaviour, the fabricated sensor can be used for the efficient determination of PRC in pharmaceutical and biological samples in future. Furthermore, the proposed synthesis method is simple, fast, large scale

production, robust, reproducible and does not require any sophisticated instruments. In future, the present process can be further extended for the construction of various morphologies and to check their possible applications in lithium-ion batteries, fuel cells, and photocatalysis.

Conflict of interests

There are no conflicts to declare.

REFERENCES

1. Klinbumrung T, Thongtem S. Characterization and gas sensing properties of CuO synthesized by DC directly applying voltage. Appl Surf Sci. 2014;313:640-6.
2. El-Trass A, ElShamy H, El-Mehasseb I, El-Kemary M. CuO nanoparticles: synthesis, characterization, optical properties and interaction with amino acids. Appl Surf Sci. 2012;258:2997-3001.
3. Kumar SK, Suresh S, Murugesan S, Raj SP. CuO thin films made of nanofibers for solar selective absorber applications. Sol Energy. 2013;94:299-304.
4. Rokhmat M, Wibowo E, Khairurrijal S, Abdullah M. Performance improvement of TiO_2/CuO solar cell by growing copper particle using fix current electroplating method. Proc Eng. 2017;170:72-7.
5. Palpandi K, Eswaran K, Kavitha B, Karthiga R, Rajarajan M, Suganthi A. Novel sphere CuO/Ag_3PO_4 nanocomposites with enhanced visible light photocatalytic activity for degradation of amaranth.
6. Karuppaiah P, Gowthaman NSK, Balakumar V, Shankar S, Lim HN. Ultrasonic synthesis of CuO nanoflakes: A robust electrochemical scaffold for the sensitive detection of phenolic hazard in water and pharmaceutical samples. Ultrason Sonochem. 2019;58:104649.
7. Zhu L, Chen Y, Sun Y, Cui Y, Liang M, Zhao J, et al. Phase-manipulable synthesis of Cu-based nanomaterials using ionic liquid 1-butyl-3-methylimidazole tetrafluoroborate. Cryst Res Technol. 2010;45:398-404.
8. Wang YQ, Meng DW, Liu XQ, Li F. Facile synthesis and characterization of hierarchical CuO nanoarchitectures by a simple solution route. Cryst Res Technol. 2009;44:1277-83.
9. Xu CK, Lin YK, Wang GH. Preparation and characterization of CuO nanorods by thermal decomposition of CuC_2O_4 precursor. Mater Res Bull. 2002;37:2365-72.
10. Jiang XC, Herricks T, Xia YN. CuO nanowires can be synthesized by heating copper substrates in air. Nano Lett. 2002;2:1333-8.
11. Palpandi K. Facile synthesis and characterization of nanowire-like copper oxide electrodes for sensitive electrochemical sensing of paracetamol [Internet]. 2025 [cited 2025 Aug 2]. Available from: https://doi.org/10.5281/zenodo.15643177
12. Ke FS, Huang L, Wei GZ, Xue LJ, Li JT, Zhang B, et al. One-step fabrication of CuO nanoribbons array electrode and its excellent lithium storage performance. Electrochim Acta. 2009;54:5825-9.
13. Ma CY, Zhu LJ, Chen SF, Zhao YX. Simple and rapid preparation of CuO nanowires and their optical properties. Mater Lett. 2013;108:114-7.
14. Sonia S, Jayram ND, Kumar PS, Mangalaraj D, Ponpandian N, Viswanathan C. Effect of NaOH concentration on structural, surface and antibacterial activity of CuO nanorods synthesized by direct sonochemical method. Superlattices Microstruct. 2014;66:1-9.
15. Shrestha KM, Sorensen CM, Klabunde KJ. Synthesis of CuO nanorods, reduction of CuO into Cu nanorods, and diffuse reflectance measurements in the near IR region. J Phys Chem C. 2010;114:14368-76.
16. Patel VK. Sonoemulsion synthesis of long CuO nanorods with enhanced catalytic thermal decomposition of potassium perchlorate. J Clust Sci. 2013;24:82-8.
17. Xiao HM, Zhu LP, Liu XM, Fu SY. Anomalous ferromagnetic behavior of CuO nanorods synthesized via hydrothermal method. Solid State Commun. 2007;141:431-5.
18. Huang JR, Fu GJ, Shi CC, Wang XY, Zhai MH, Gu CP. Novel porous CuO microrods: synthesis, characterization, and photocatalysis property. J Phys Chem Solids. 2014;75:1011-6.
19. Bayansal F, Cetinkara HA, Kahraman S, Cakmak HM, Guder HS. Nano-structured CuO films prepared by simple solution methods: plate-like, needle-like and network-like architectures. Ceram Int. 2012;38:1859-66.
20. Zhang Y, He XL, Li JP, Zhang HG, Gao XG. Gas-sensing properties of hollow and hierarchical copper oxide microspheres. Sens Actuators B Chem. 2007;128:293-8.
21. Yang LX, Zhu YJ, Tong H, Li L, Zhang L. Multistep synthesis of CuO nanorod bundles and interconnected nanosheets using Cu2(OH)3Cl plates as precursor. Mater Chem Phys. 2008;112:442-7.
22. Ba N, Zhu L, Zhang G, Li J, Li H. Facile synthesis of 3D CuO nanowire bundle and its excellent gas sensing and electrochemical sensing properties. Sens Actuators B. 2016;227:142-8.
23. Gao F, Zhu L, Li H, Xie H. Hierarchical flower-like CuO film: One-step room temperature synthesis, formation mechanism and excellent optoelectronic properties. Mater Res Bull. 2017;93:342-51.
24. Xie H, Zhu L, Zheng W, Zhang J, Gao F, Wang Y. Microwave-assisted template-free synthesis of butterfly-like CuO through Cu2Cl(OH)3 precursor and the electrochemical sensing property. Solid State Sci. 2016;61:146-54.
25. Wade A. Martindale: The Extra Pharmacopoeia. 27th ed. London: The Pharmaceutical Press; 1979.
26. Prabakar SJR, Narayanan SS. Amperometric determination of paracetamol by a surface modified cobalt hexacyanoferrate graphite wax composite electrode. Talanta. 2007;72:1818-27.

27. Fogg AG, Sausins PJ, Smithson JR. The determination of paracetamol and aspirin in mixtures by nonaqueous potentiometric titrimetry or by ultraviolet spectrophotometry. Anal Chim Acta. 1970;49:342-5.
28. Brandt K. Paracetamol in the treatment of osteoarthritis pain. Drugs. 2003;63:23-41.
29. Li J, Liu J, Tan G, Jiang J, Peng S, Deng M, et al. High-sensitivity paracetamol sensor based on Pd/graphene oxide nanocomposite as an enhanced electrochemical sensing platform. Biosens Bioelectron. 2014;54:468-75.
30. Kesavan S, John SA. Stable determination of paracetamol in the presence of uric acid in human urine sample using melamine grafted graphene modified electrode. J Electroanal Chem. 2016;760:6-14.
31. Gowda JI, Gunjiganvi DG, Sunagar NB, Bhat MN, Nandibewoor ST. MWCNT–CTAB modified glassy carbon electrode as a sensor for the determination of paracetamol. RSC Adv. 2015;5:49045-53.
32. Mao A, Li H, Jin D, Yu L, Hu X. Fabrication of electrochemical sensor for paracetamol based on multi-walled carbon nanotubes and chitosan–copper complex by self-assembly technique. Talanta. 2015;144:252-7.
33. Montaseri H, Forbes PBC. Analytical techniques for the determination of paracetamol: A review. TrAC Trends Anal Chem. 2018;108:122-34.
34. Lecoeur M, Rabenirina G, Schifano N, Odou P, Ethgen S, Lebuffe G, et al. Determination of paracetamol and its main metabolites in urine by capillary electrophoresis hyphenated to mass spectrometry. Talanta. 2019;205:120108.
35. Glavanović S, Glavanović M, Tomišić V. Simultaneous quantitative determination of paracetamol and tramadol in tablet formulation using UV spectrophotometry and chemometric methods. Spectrochim Acta A Mol Biomol Spectrosc. 2016;157:258-64.
36. Chaves SC, Aguiar PNC, Torres LMFC, Gil ES, Luz RCS, Damos FS, et al. Simultaneous determination of caffeine, ibuprofen, and paracetamol by flow-injection analysis with multiple-pulse amperometric detection on boron-doped diamond electrode. Electroanalysis. 2015;27:2785-91.
37. Jeevagan AJ, John SA. Electrochemical determination of caffeine in the presence of paracetamol using a self-assembled monolayer of non-peripheral amine substituted copper (II) phthalocyanine. Electrochim Acta. 2012;77:137-42.
38. Kalimuthu P, John SA. Selective electrochemical determination of paracetamol using nanostructured film of functionalized thiadiazole modified electrode. Electroanalysis. 2010;22:303-9.
39. Kutluay A, Aslanoglu M. An electrochemical sensor prepared by sonochemical one-pot synthesis of multi-walled carbon nanotube-supported cobalt nanoparticles for the simultaneous determination of paracetamol and dopamine. Anal Chim Acta. 2014;839:59-66.
40. Biswas S, Chakraborty D, Das R, Bandyopadhyay R, Pramanik P. A simple synthesis of nitrogen doped porous graphitic carbon: Electrochemical determination of paracetamol in presence of ascorbic acid and p-aminophenol. Anal Chim Acta. 2015;890:98-107.
41. Wu XY, Niu WJ, Cosnier S, Deng SY, Zhang XJ, Shan D. Ferricyanide confined into the integrative system of pyrrolic surfactant and SWCNTs: The enhanced electrochemical sensing of paracetamol. Electrochim Acta. 2015;186:16-23.
42. Shrestha S, Liu Y, Mustain WE. Electrocatalytic activity and stability of Pt clusters on state-of-the-art supports: a review. Catal Rev. 2011;53(3):256-336.
43. International Centre for Diffraction Data (ICDD), Joint Committee on Powder Diffraction Standards. Diffraction Data File No. 05-0661. 2000;12.
44. Ansari MA, Jahan N. Structural and optical properties of BaO nanoparticles synthesized by facile co-precipitation method. Mater Highl. 2021;2(1):23-8.
45. Karuppaiah P, Gowthaman NSK, Balakumar V, Shankar S, Lim HN. Ultrasonic synthesis of CuO nanoflakes: A robust electrochemical scaffold for the sensitive detection of phenolic hazard in water and pharmaceutical samples. Ultrason Sonochem. 2019;58:104649.
46. Jin S, Hao Z, Zhang K, Yan Z, Chen J. Advances and challenges for the electrochemical reduction of CO_2 to CO: from fundamentals to industrialization. Angew Chem. 2021;133(38):20795-20816.
47. Shigehara K, Anson FC. Electrocatalytic activity of three iron porphyrins in the reductions of dioxygen and hydrogen peroxide at graphite electrodes. J Phys Chem. 1982;86(14):2776-83.
48. Zuo Y, Sheng W, Tao W, Li Z. Direct methanol fuel cells system – A review of dual-role electrocatalysts for oxygen reduction and methanol oxidation. J Mater Sci Technol. 2022;114:29-41.
49. Arvand M, Gholizadeh TM. Simultaneous voltammetric determination of tyrosine and paracetamol using a carbon nanotube-graphene nanosheet nanocomposite modified electrode in human blood serum and pharmaceuticals. Colloids Surf B. 2013;103:84-93.
50. Kang X, Wang J, Wu H, Liu J, Aksay IA, Lin Y. A graphene-based electrochemical sensor for sensitive detection of paracetamol. Talanta. 2010;81:754-9.
51. Lourenção BC, Medeiros RA, Rocha-Filho RC, Mazo LH, Fatibello-Filho O. Simultaneous voltammetric determination of paracetamol and caffeine in pharmaceutical formulations using a boron-doped diamond electrode. Talanta. 2009;78:748-52.
52. Kachoosangi RT, Wildgoose GG, Compton RG. Sensitive adsorptive stripping voltammetric determination of paracetamol at multiwalled carbon nanotube modified basal plane pyrolytic graphite electrode. Anal Chim Acta. 2008;618:54-60.
53. Keeley GP, McEvoy N, Nolan H, Kumar S, Rezvani E, Holzinger M, et al. Simultaneous electrochemical determination of dopamine and paracetamol based on thin pyrolytic carbon films. Anal Methods. 2012;4:2048-53.

54. Huang KJ, Wang L, Li J, Liu YM. Electrochemical sensing based on layered MoS_2–graphene composites. Sens Actuators B Chem. 2013;178:671-7.
55. Yin H, Shang K, Meng X, Ai S. Voltammetric sensing of paracetamol, dopamine and 4-aminophenol at a glassy carbon electrode coated with gold nanoparticles and an organophilic layered double hydroxide. Microchim Acta. 2011;175:39-45.
56. Xiong H, Xu H, Wang L, Wang S. Characterization and sensing properties of a carbon nanotube paste electrode for paracetamol. Microchim Acta. 2009;167:129-33.
57. Wang SF, Xie F, Hu RF. Carbon-coated nickel magnetic nanoparticles modified electrodes as a sensor for determination of paracetamol. Sens Actuators B Chem. 2007;123:495-500.
58. Fan Y, Liu JH, Lu HT, Zhang Q. Electrochemical behavior and voltammetric determination of paracetamol on Nafion/TiO_2–graphene modified glassy carbon electrode. Colloids Surf B. 2011;85:289-92.
59. Li MQ, Jing LH. Electrochemical behavior of paracetamol and its detection on the PANI–MWCNTs composite modified electrode. Electrochim Acta. 2007;52:3250-7.
60. Shetti NP, Malode SJ, Nayak DS, Aminabhavi TM, Reddy KR. Nanostructured silver doped TiO_2/CNTs hybrid as an efficient electrochemical sensor for detection of anti-inflammatory drug, cetirizine. Microchem J. 2019;150:104124.
61. He B, Liu H. Electrochemical determination of nitrofuran residues at gold nanoparticles/graphene modified thin film gold electrode. Microchem J. 2019;150:104108.
62. Rezvani SA, Soleymanpour A. Application of a sensitive electrochemical sensor modified with WO_3 nanoparticles for the trace determination of theophylline. Microchem J. 2019;149:104005.
63. Laviron E. General expression of the linear potential sweep voltammogram in the case of diffusionless electrochemical systems. J Electroanal Chem. 1979;101:19-28.
64. Jalili H, Aslibeiki B, Varzaneh AG, Chernenko VA. The effect of magneto-crystalline anisotropy on the properties of hard and soft magnetic ferrite nanoparticles. Beilstein J Nanotechnol. 2019;10:1348-59.
65. Wang MY, Xu Y, Chen S, Ye MF, Li ZK, Fan H, et al. Accurate electrochemical paracetamol sensor for drug control through catalytic roles of single Fe atoms. Rare Metals. 2025;1-11.
66. Yu W, Xu X, Cao T, Wei Z, Tang J, Zhang M. Laser-induced graphene/gold nanoparticle hybrid sensor for enhanced electrochemical detection of paracetamol. Anal Methods. 2024;16(44):7527-33.
67. Liu XL, Guo JW, Wang YW, Wang AZ, Yu X, Ding LH. A flexible electrochemical sensor for paracetamol based on porous honeycomb-like NiCo-MOF nanosheets. Rare Metals. 2023;42(10):3311-7.
68. Allende S, Liu Y, Jacob MV. Electrochemical sensing of paracetamol based on sugarcane bagasse-activated biochar. Ind Crops Prod. 2024;211:118241.

About the Corresponding Author

Palpandi Karuppaiah, from Vadasithur, Tamil Nadu, is a researcher specializing in nanomaterials and electrochemical sensors, known for developing CuO-based catalysts for paracetamol detection in biological samples.